# Chapter 7
# Electron Microscopy Techniques

**Marijn A. van Huis and Heiner Friedrich**

**Abstract** This chapter introduces the basic concepts of electron microscopy, which comprises an extensive toolbox for characterizing the size, three-dimensional shape, composition, and crystal structure of nanoparticles, nanoparticle superstructures and nanostructured materials.

## 7.1 Introduction: Imaging Nanoparticles with Electrons

The most characteristic property of nanoparticles (NPs) is their nanoscale size. It is this small scale that results in interesting physical properties (optical, magnetic, electronic, opto-electronic, etc.), which differ from the properties of their bulk counterparts (see Chap. 1). The simple fact that the particles are of nanometer size renders observation by light microscopy impossible, as the dimensions of the NPs are much smaller than the typical wavelength of light (hundreds of nanometers). Therefore, electrons—which have a much smaller wavelength than light—are much better suited to study the structural properties of NPs. Nowadays, electron microscopes (EM) are available with a spatial resolution of 50 pm, which is considerably smaller than the typical distance between atoms (200 pm or 2 Å). Because of this superior resolution, the structure of surfaces and interfaces of NPs can now be imaged with atomic resolution. As the incident electrons interact with the atoms in the sample in very diverse ways (scattering, diffraction, electron energy losses, induced X-ray emission), a large variety of methods and techniques have been developed that can be used to obtain additional information on the material under

M.A. van Huis
Soft Condensed Matter, Debye Institute for Nanomaterials Science, Utrecht University, Princetonplein 5, 3584 CC Utrecht, The Netherlands

H. Friedrich (✉)
Laboratory of Materials and Interface Chemistry, Eindhoven University of Technology, P.O. Box 513, 5600 MB Eindhoven, The Netherlands
e-mail: h.friedrich@tue.nl



C. de Mello Donegá (ed.), *Nanoparticles*,
DOI 10.1007/978-3-662-44823-6_7

study. In this chapter we provide only a brief overview of the most commonly used methods. The book *Transmission Electron Microscopy—A Textbook for Materials Science* by D.B. Williams and C.B. Carter [1] can be found in EM facilities all over the world and provides a very comprehensive introduction to the field. A very complete overview of EM is given in the *Handbook of Nanoscopy*, edited by G. van Tendeloo et al. [2]. It should be stressed that one can learn electron microscopy only by spending many hours behind the microscopes in a continuous effort to obtain the best images possible. Finally, it is strongly recommended to collaborate with experienced electron microscopists for the interpretation of the data. *What you see is not always what you get*: the way the image looks depends strongly on the settings of the microscope, and the interpretation of images is sometimes far from trivial.

In the next Sect. 7.2 we will explain the distinction between scanning electron microscopy (SEM) and transmission electron microscopy (TEM). While SEM can be used to study large, micrometer scale assemblies of NPs, TEM is mostly used to analyze individual NPs and smaller assemblies because of its superior resolution. We will conclude Sect. 7.2 with some remarks on sample preparation.

In the remainder of this Chapter, the main imaging modes of the TEM instrument will be discussed: regular TEM imaging, and *scanning* transmission electron microscopy (STEM) (Sect. 7.3). We will then proceed to describe at a basic level the most important interaction mechanisms of electrons with matter: ***electron diffraction*** (Sect. 7.4), and scattering events which enable a number of viewing modes (Sect. 7.5). To bring relief to the restriction that conventionally only two-dimensional images are recorded, we will discuss ***electron tomography*** in Sect. 7.6, a method which allows three-dimensional reconstruction of NPs and their assemblies. In Sect. 7.7 ***analytical TEM*** will be described as a means to map the local chemical composition of the NPs. The study of particles and molecules in liquids, and of very soft materials, in general requires *cryo-TEM*, whereby the sample is analyzed at liquid nitrogen temperatures ($\sim$77 K). This technique is discussed in Sect. 7.8. Finally, in Sect. 7.9 we discuss **in situ *TEM***: performing experiments such as heating and gas exposure inside the electron microscope, before concluding with some general remarks on future developments (Sect. 7.10).

## 7.2 Scanning Electron Microscopy (SEM) and Transmission Electron Microscopy (TEM)

The basic scheme of the SEM and TEM setups and representative images are shown in Fig. 7.1. In ***Scanning Electron Microscopy*** (SEM), the acquired image is built up from electrons that are reflected (backscattered electrons, BSE) or emitted (secondary electrons, SE) from the surface of the material under investigation. The electron beam is focused into an electron probe, which is scanned over the surface in a raster scan pattern. Therefore, the pixels in a SEM image originate from electrons that are collected sequentially point by point in a detector (usually an

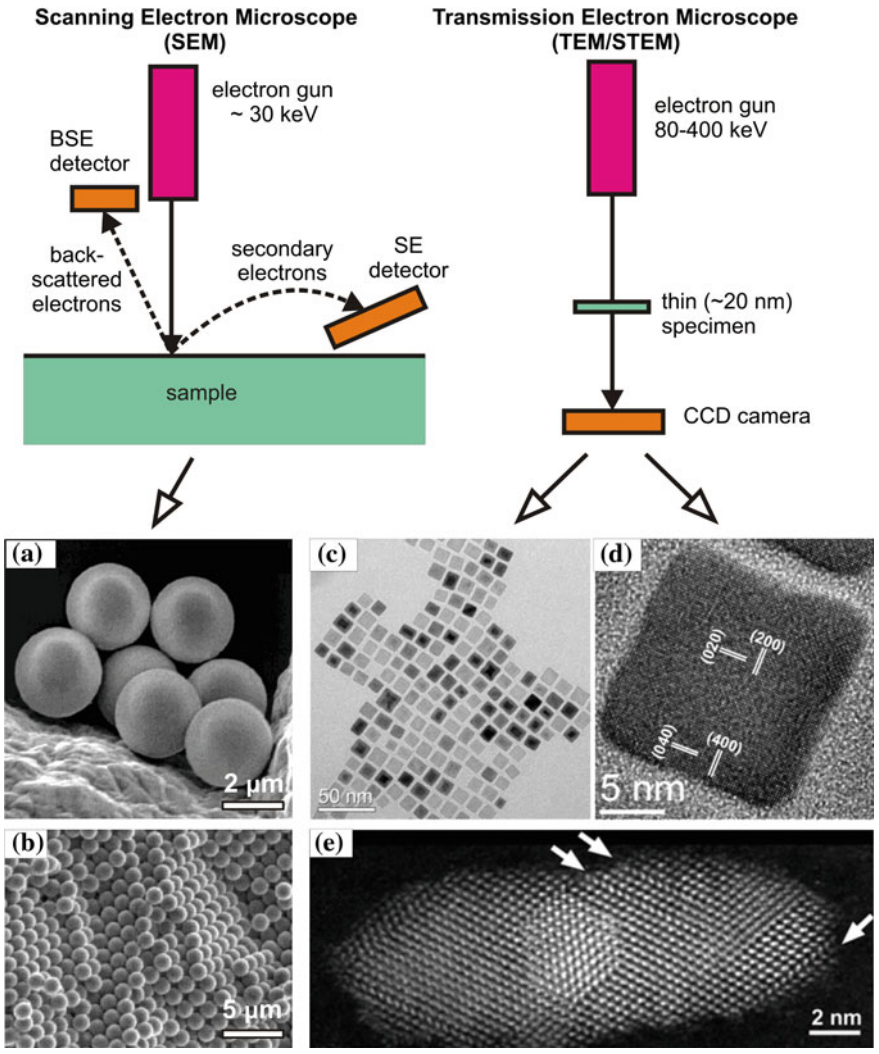


**Fig. 7.1** *Top* schematic showing the basic principle of scanning and transmission electron microscopes (SEM and TEM, respectively). Images recorded in the SEM display surfaces. **a** ZnS NPs on a support. **b** Silica NPs assembled in a superstructure. TEM imaging provides two-dimensional projections of the NPs. **c** Deposited cubical $FeO_x/CoFe_2O_4$ core/shell NPs. **d** High-resolution image of a NP in **c** with atomic planes indicated. **e** High-resolution HAADF-STEM image of a CdSe rod shell with a faceted PbSe core at the centre. Images **c**, **d**: courtesy of Yalcin et al. [3]. Image **a** is reprinted with permission from Ref. [4]. Copyright (2001) American Chemical Society. Image **e** is reprinted with permission from Ref. [5]. Copyright (2011) American Chemical Society

Everhart-Thornley detector). Alternatively, nanostructures can be imaged in transmission mode using ***Transmission Electron Microscopy*** (TEM), whereby the electrons travel through a very thin sample (usually called a *specimen*) and are collected by a detector at the rear side. The latter method requires that the specimen is very thin (it should be *electron-transparent*, typically less than 100 nm thick). Using SEM, one obtains an image of the *surface* of the nanomaterial. Using TEM, one obtains a *two-dimensional projection* of the nanomaterial. There are many other microscopy techniques such as scanning tunneling microscopy (STM, Chap. 8), atomic force microscopy (AFM, Chap. 8), electron probe microscopic analysis (EPMA), correlative light and electron microscopy (CLEM), and X-ray microscopy (XRM), which will not be discussed here. In the remainder of this chapter, we will discuss almost exclusively TEM, because of its superior resolution which allows extracting very detailed information from nanoscale samples.

### *7.2.1 Specimen Preparation Techniques*

Many NPs are synthesized under wet chemistry conditions (see Chap. 6) and are therefore dispersed in solvents (colloidal suspensions). In case the NPs are stable without the solvent, no special sample preparation is required for TEM investigation. When the NPs are sufficiently diluted, dropcasting of one drop of the suspension onto a TEM support film such as a thin carbon foil, followed by evaporation of the liquid medium, is sufficient for basic imaging. Alternatively, the TEM grid may be dipped for a few seconds in the NP suspension. In general, 'washing' the suspended NPs (i.e., removing excess surfactants and other molecules) prior to dropcasting is highly recommended. This can be achieved by precipitating the NPs from the colloidal suspension by addition of a non-solvent, followed by centrifugation and redispersion of the NPs in a solvent (this purification process may be repeated several times). Sometimes high-quality imaging of the NPs is hampered by the presence of ligands at the surface, or by other molecules that were present in the colloidal suspension. In those cases, a fast 5–30 s plasma etch (the plasma typically consists of Ar and O ions) is applied to remove the molecules which were blurring the images. Much precaution should be taken not to modify the NPs in the process.

There are cases where a more extensive sample preparation is required. For example, in the case of catalytic NPs that are present in much larger three-dimensional porous supports, in the case of multilayer semiconductor quantum dot films (solar cell nanomaterials), and when studying three-dimensional self-ordered NP assemblies (Fig. 7.1b). In those cases, the conventional materials science techniques of grinding, polishing, and ion milling (i.e., sputtering atoms from the sample at a low incident angle using a 4 keV $Ar^+$ ion beam) can provide electron-transparent samples. On the other hand, most 3D nanoparticle materials are rather soft, and will not withstand conventional grinding and polishing. In those cases, a more advanced technique is FIB-SEM (focused ion beam inside the scanning

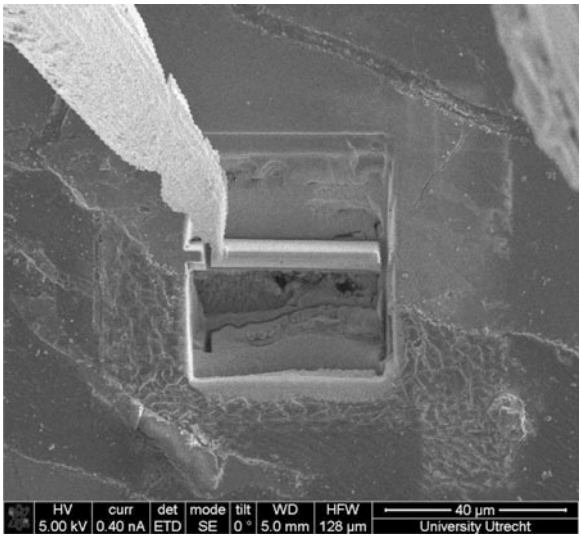


**Fig. 7.2** Scanning electron microscope (SEM) image showing a trench in the surface of geological rock material, with at the center the lamella that has been cut out using a focused ion beam (FIB) of $Ga^+$ ions. The lamella is attached to a needle by ion-induced Pt deposition at the contact point, and is subsequently cut completely free from the trench and transported and deposited onto a TEM support using the needle (courtesy of C.T.W.M. Schneijdenberg, Utrecht University)

electron microscope), whereby a focused $Ga^+$ ion beam is used to cut out a very thin slice (called a 'lamella') out of a larger sample. An example is shown in Fig. 7.2. This slice (with a typical thickness of 20–50 nm) can then be further analyzed in the TEM.

## 7.3 Two Imaging Modes: TEM and STEM

There are two main imaging modes of the transmission electron microscope. When imaging in the regular TEM mode, a wide, homogeneous and parallel electron beam is incident on the sample as indicated schematically at the left-hand side of Fig. 7.3. Alternatively, the electron beam can be focused into a fine spot (50–1,000 pm wide, depending on the microscope) at the position of the specimen, whereby one speaks of an *electron probe*. This probe beam is then scanned over the surface of the specimen in a matrix of e.g. 1,000 × 1,000 points in X and Y direction, whereby the image is created point by point. Hence, this operational mode is called *scanning transmission electron microscopy* (STEM). Underneath the specimen, a ring-shaped detector is placed that collects only electrons that have undergone a scattering event, so that they do not proceed along the central optical axis, but are scattered at an angle large enough to hit the ring. By varying the angle of the edges

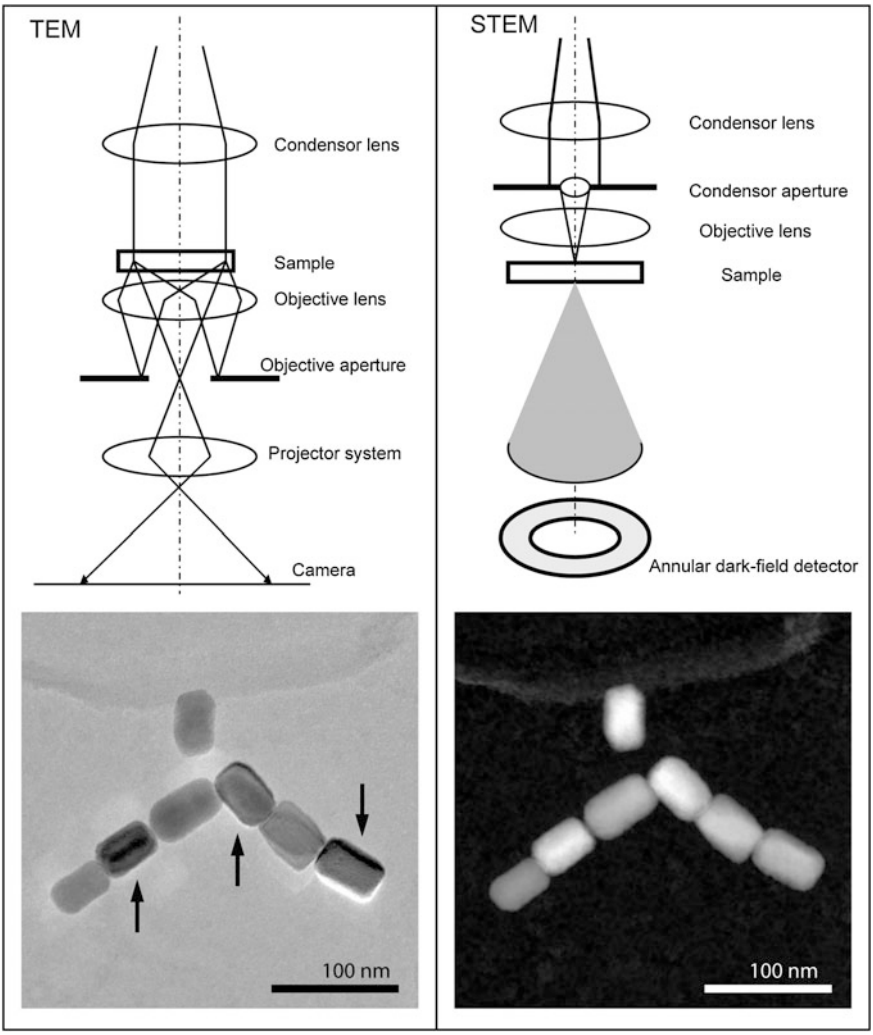


**Fig. 7.3** Ray diagram for *bright-field* TEM and annular *dark-field* STEM mode with examples of $Fe_3O_4$ NPs imaged in the corresponding mode shown below. The *arrows* in the TEM image denote NPs that have their crystal lattice aligned with the electron beam resulting in bright 'ghosts'. The lenses consist of electromagnetic fields that control and focus the electron beam

of the ring with respect to the optical axis, electrons can be selected that have interacted with very heavy atoms (strong scattering, large scattering angle), or that have interacted with lighter atoms (smaller scattering angle).

Below the ray diagrams in Fig. 7.3 example images of the two imaging modes are given, in which $Fe_3O_4$ NPs on top of a thin carbon support membrane are imaged. In the TEM image the NPs appear darker than the support, because the heavier NPs will "stop" (scatter or diffract) a number of the incident electrons, so

that they are not detected on the camera behind the specimen. In annular dark field (ADF) STEM mode, the carbon support appears dark. Carbon is a very light element that hardly scatters electrons. The electrons that interact with the carbon atoms, will hardly be deflected and will thus proceed in a forward trajectory, passing through the center of the ring (right side in Fig. 7.3), so that they are not detected at all. The electrons that are detected on the ring-shaped ADF detector, almost all originate from interactions with the $Fe_3O_4$ NPs, which is why they appear bright in the ADF-STEM image.

One should always realize that in regular TEM mode with the wide parallel beam, all electrons that contribute to the image are collected in principle simultaneously (although there is always a finite exposure time). In STEM mode, the image is created sequentially, pixel by pixel, by scanning the electron probe across the sample, so that the acquisition of a STEM image takes more time (e.g., 5 s for STEM vs. 1 s for TEM). Therefore, STEM recording is more sensitive to drift of the specimen (due to, e.g., mechanical vibrations and temperature variations). The advantages and disadvantages of various viewing modes, and the underlying physical mechanisms, will be discussed more extensively in Sects. 7.4 and 7.5.

## 7.4 Electron Diffraction

When analyzing NPs and their assemblies it is in some cases desirable not to look at a magnified image of the sample, but instead, at the pattern generated in the back-focal plane (BFP) of the objective lens. The BFP of the objective lens is the plane in which the objective aperture (OA) is located. Note that in electron diffraction the OA is withdrawn from the beam path. For almost all specimens, and in particular for specimens made up of regularly spaced arrays of atoms, the intensity distribution in the BFP is inhomogeneous, often showing a pattern of spots or rings. These patterns, referred to as ***electron diffraction patterns***, arise from the interaction of a parallel and coherent beam of electrons with an ordered (e.g. polycrystalline) sample by interference of the refracted electron waves from neighboring atoms and lattice planes. The diffraction pattern (DP) generated in the BFP can be viewed magnified on screen or recorded on the CCD camera by suitably focused transfer and projection lenses. Since the DP is generated from the entire area that is illuminated by the electron beam, the information from many NPs is averaged. To differentiate between the DP generated in different regions or from different NPs an aperture, referred to as selected area electron diffraction (SAED) aperture can be inserted in the beam path (see Fig. 7.4).

The position of the rings or spots in a diffraction pattern (DP) with respect to the central beam gives information on the specimens atomic scale order, such as being amorphous, poly- or single- crystalline, including the respective lattice parameters and symmetry, grain morphology, grain-size distribution, or grain orientation. Nevertheless, a detailed analysis can be time consuming and often requires the combination of electron diffraction with atomic resolution images. In this context, it

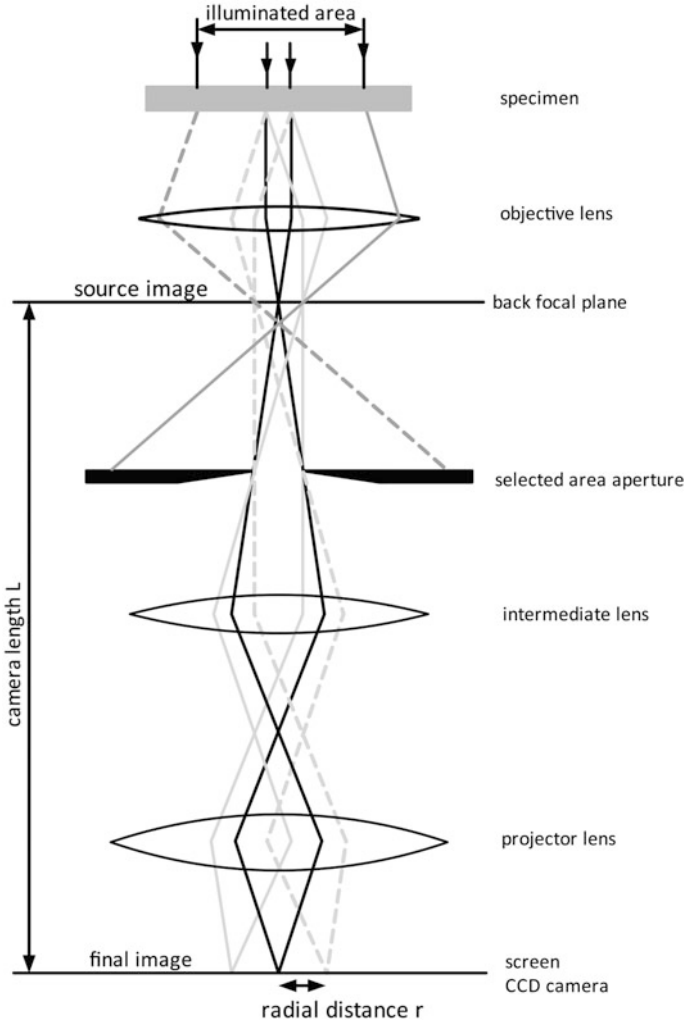


**Fig. 7.4** Ray diagram for selected area electron diffraction (SAED)

suffices to say that the radial distance of the rings or spots can be evaluated in terms of lattice distances similar to X-ray diffraction. The *lattice distance* ($d = \lambda \cdot L/r$) is related to the radial distance ($r$ in mm) by the wavelength of the electrons ($\lambda = 3.86$ pm for 100 kV and $\lambda = 2.54$ pm for 200 kV acceleration voltage) and the camera length ($L$ in mm, distance between the scattering event and the recording plane).

An example illustrating electron diffraction without and with a selected area aperture on assemblies of magnetite NPs is shown in Fig. 7.5. Note that the illuminated area in Fig. 7.5a is much larger than the area of the image. Illuminating and, thus, averaging over a large number of NPs (Fig. 7.5a) leads to a DP consisting

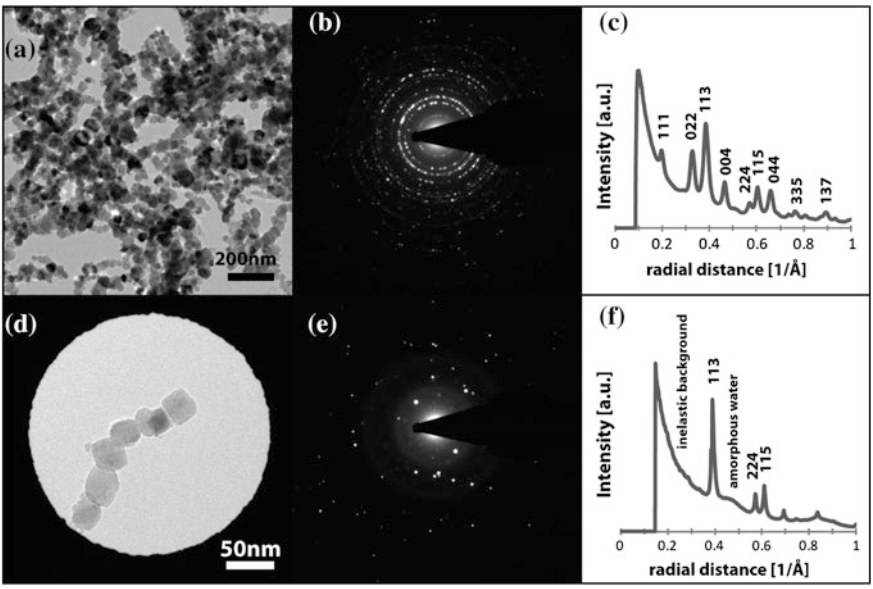


**Fig. 7.5** Image (**a**, **d**), diffraction pattern (**b**, **e**) and radial average (**c**, **f**) of $FeO_x$ NPs without (**a–c**) and with (**d–f**) selected area electron diffraction (SAED) aperture [6]

of rings (Fig. 7.5b) which is, if radially averaged (Fig. 7.5c), comparable in information to a powder X-ray diffraction pattern. In case a SAED aperture is inserted in the beam path (Fig. 7.5d) the information in the DP is limited to the magnetite NP within the field of view, thus, no rings but only diffraction spots (Fig. 7.5e) are visible. Henceforth, the radial average of the spot pattern plotted in (Fig. 7.5f) differs from the that shown in Fig. 7.5c and may indicate preferential orientation of the NPs on the TEM grid on account of e.g. shape anisotropy. The increase in background signal towards low radial distances results from inelastic interactions between electron beam and sample. In the limit of only one crystallite being present in the selected field of view its crystalline lattice and orientation with respect to the electron beam can be determined. If one carefully examines Fig. 7.5e, two diffuse rings are observed. The rings are caused by the fact that the NPs were imaged in a vitreous water layer, a technique referred to as Cryo-TEM which will be further discussed in Sect. 7.8. The position and breadth of the broad maximum at a radial distance of $\sim 4.7$ Å$^{-1}$ corresponding to $\sim 2.1$ Å nearest neighbor distance is a characteristic of amorphous, i.e. vitreous, water.

To complete the discussion of electron diffraction, it needs to be added that it also can be carried out using a convergent (S)TEM probe. In convergent beam electron diffraction (CBED) the diffraction spots widen to discs containing additional bright and dark features. Henceforth, CBED provides beyond unit cell and associated lattice parameters, also quantitative data on specimen thickness, lattice-strain (key parameters for semiconductors and other multilayer nanostructures),

valence-electron distribution, or chemical bonding. However, this information can only be extracted aided by detailed CBED pattern simulations.

In summary, electron diffraction complements X-ray diffraction providing detailed crystallographic information of small volumes such as individual NPs (electron-matter interaction is about 1 million times stronger than x-ray-matter interactions) and with exposure times in the order of seconds (much longer exposures are needed for X-rays, except when using high brightness synchrotron sources).

## 7.5 Advanced Imaging—Contrast Modes

As explained in Sect. 7.3, electron microscopes are operated in two basic modes, TEM or STEM. To understand the information contained in the corresponding images it is worthwhile to look at the electron-sample interaction and how image contrast is generated. As shown in Fig. 7.6a, in TEM a parallel beam of electrons may be transmited through a sample consisting of a low and a high mass-density region. The high-density region will interact more strongly with the electron beam and, thus, scatter more of the incoming electrons. Electrons scattered towards the objective aperture are removed from the beam resulting in lower image intensity in the corresponding image region. This contrast mode is referred to as ***mass-contrast*** and occurs for homogeneously thick samples. It can be used to distinguish same-sized NPs with vastly different elemental compositions, e.g. carbon or metal NPs. It is also applied to image organic macromolecules by embedding them in a homogeneously thick film of a heavy metal stain. The stain creates a strongly scattering replica of the macromolecules outline, thus enhancing contrast.

Besides differences in mass-density, differences in thickness, as shown in Fig. 7.6b, also generate contrast. ***Thickness contrast*** results in a reduced image intensity of thick sample regions, thus providing information such as surface roughness, or object outline. Note that a (S)TEM image is in first approximation a two dimensional (2D) projection of a 3D object along the beam path. Henceforth, image intensities reflect the cumulative thickness of objects. The contrast effects discussed above are commonly combined into ***mass-thickness-contrast,*** which is quite similar to the well-known Lambert-Beer absorption contrast. However, it is only virtual absorption by the objective aperture creating TEM contrast, which is increasing with decreasing aperture size. The recorded image intensity $(I \sim I_0 e^{-\sigma t})$ scales with the total (in) elastic scattering cross-section ($\sigma$) and the sample thickness ($t$).

In case of crystalline NPs, image contrast will also depend on the orientation of the crystal lattice with respect to the electron beam. As illustrated in Fig. 7.6c, if lattice planes of a NP are parallel to the electron beam the diffraction pattern generated in the back focal plane of the objective lens will contain strong diffraction spots. If these spots are cut out by a suitably sized objective aperture the image intensity of the oriented NP will be significantly decreased, which is referred to as ***diffraction contrast***. All crystalline NPs with non-parallel orientation and all amorphous NPs will not show this behavior. Based on above contrast considerations

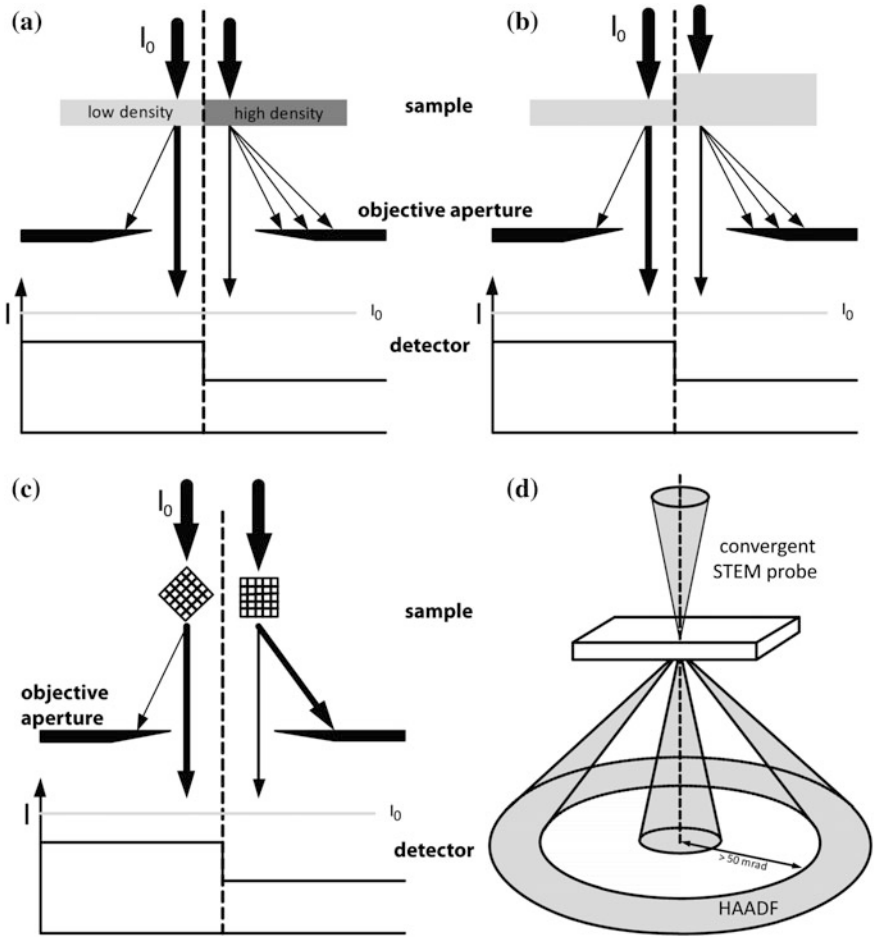


**Fig. 7.6** Cartoon of contrast generation by mass-density (**a**); thickness (**b**); crystal orientation (**c**); and atomic number (**d**)

one can easily infer that in general it is difficult to distinguish between dense, thick or oriented crystalline NPs using a single TEM image.

To simplify the intricate contrast associated with the coherent nature of electron waves, i.e. the scattering of electrons into low angles, a technique called ***z-contrast imaging*** is utilized. It employs a convergent STEM probe that transverses the sample as sketched in Fig. 7.6d. The image is formed point by point using only electrons that are scattered into angles larger than 50 mrad onto a high-angle annular dark-field (HAADF) detector. In HAADF images the contrast is predominantly incoherent as electrons are scattered close to the atomic core which is governed by thermal vibrations. In more physical terms, the electron-matter interaction approaches the unscreened Rutherford scattering cross-section, which generates images with intensities that are proportional to the square of the atomic number of the element

($I \sim Z^2$). Note that the Rutherford limit is not reached and the exact dependence has many parameters. Overall, HAADF imaging is very little susceptible to lattice orientation effects. One significant limitation is that only a very small fraction of the impinging electrons are used for imaging, thus requiring a high initial dose. Henceforth, only beam-stable materials like e.g. (metal)oxide NPs on a carbon support film can be imaged by HAADF STEM without damage.

An example of a bright-field (BF) TEM image of biogenic magnetite ($Fe_3O_4$) NPs and a HAADF STEM image of the same chain of crystallites was displayed in Fig. 7.3 above. While the contrast of the NPs in the TEM image is strongly dependent on thickness, lattice orientation and defocus (see arrows in Fig. 7.3a for oriented crystallites), the STEM image more closely approximates a projection of the thickness along the electron trajectory.

The observation that the intensity in BF-TEM images depends on the defocus of the objective lens deserves a more detailed discussion. This requires that we leave the description of a particle beam that interacts with the sample behind and use the more general concept of electron waves that was also utilized in the previous section on electron diffraction. In wave optics the electron is described by its associated wave following de Broglie's equation, i.e. the electron wavelength ($\lambda = h/p$) is given by Planck's constant ($h$) divided by the momentum of the electron ($p$). This gives wavelengths of $\lambda = 3.86$ pm for electrons accelerated in an electric potential of 100 kV and $\lambda = 2.54$ pm for 200 kV. Furthermore, the electron wave is described not only by its wavelength but also by its amplitude ($a$) and phase ($\phi$). The interaction of an electron wave with a sample and the magnifying objective lens is sketched in Fig. 7.7.

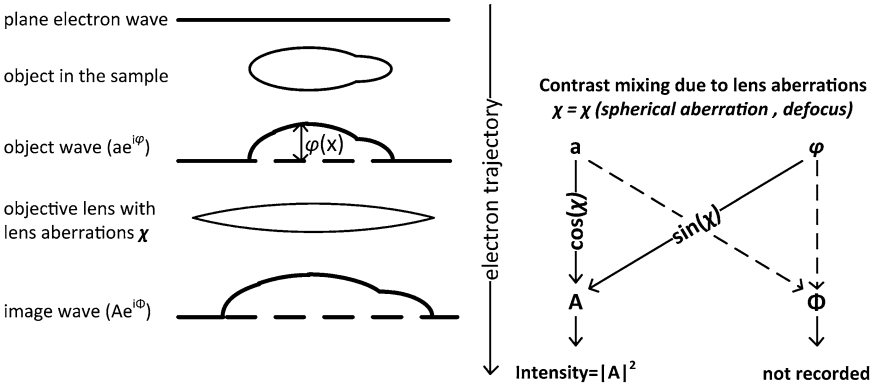


**Fig. 7.7** Scheme of electron wave optics and contrast mixing

The imaging process starts with a plane electron wave (a = 1, $\phi = 0$ everywhere) whose phase is locally deformed or 'bent' by the sample's electromagnetic potential. This process is analogous to light travelling slower in a medium with higher refractive index, such as glass, leaving the object with a modulated wave front. Most importantly for atomic resolution TEM, the resulting object wave has a position dependent phase shift $\phi(x,y)$ imprinted on it. The amplitude and phase

information contained in the object wave is then transferred and mixed by the objective lens into the image wave. The mixing of object wave information occurs on account of the objective lens aberrations (χ) with spherical aberration and defocus being the main contributors. Since intensity ($I = |A|^2$) is only recorded in the final CCD image, tuning of the ***phase contrast transfer function*** (PCTF = sin (χ)) by choosing a suitable defocus determines the information content of the image.

Figure 7.8 further illustrates the relation between defocus and image contrast by showing images of gold and silica NPs on a carbon support film. In positive focus condition (Fig. 7.8b and light gray curve in Fig. 7.8a), phase contrast is bright (positive lobe at large feature sizes), thus competing with mass-thickness (amplitude) contrast. The modulations in the PCTF act like a filter resulting in the strange appearance of the image. When decreasing the defocus, phase contrast transfer becomes inverted (negative values equals dark objects) with the first curve minimum (−1) shifted to small feature sizes needed for atomic resolution imaging. Under such conditions objects such as the silica NP are often not seen (Fig. 7.8c) while for the gold NPs mass-thickness (amplitude) contrast dominates. Defocussing further to negative values shifts the transfer band (negative lobe at large feature sizes of black curve Fig. 7.8a) to increase the contrast of the silica NPs.

To experimentally obtain an estimate of the actual defocus, one starts by finding the focus producing minimum image contrast. To improve accuracy this should be

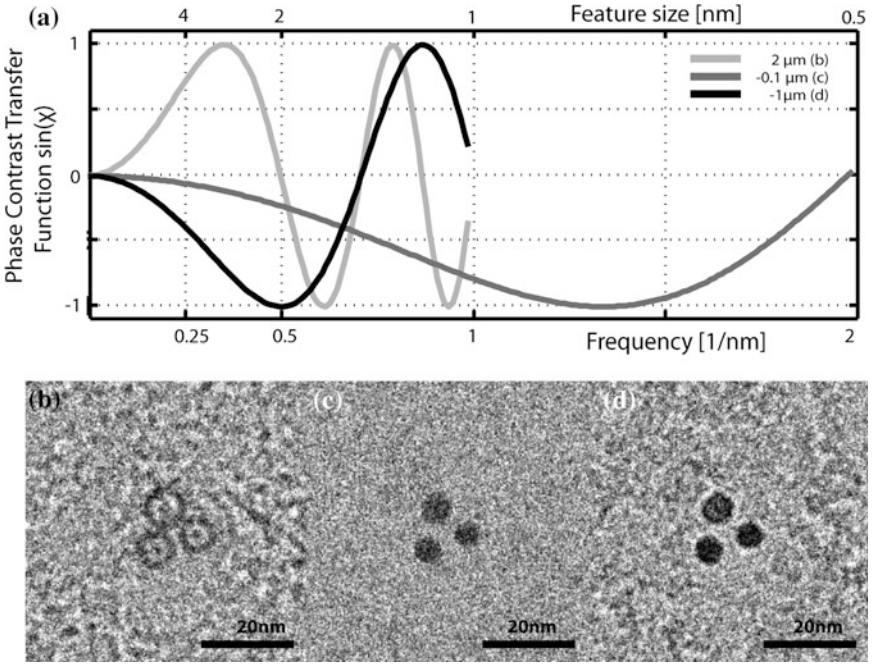


**Fig. 7.8** **a** Plot of phase contrast transfer function (PCTF) for images of gold and silica NPs on a carbon film taken at, **b** 2 μm, **c** −0.1 μm, and **d** −1 μm defocus

carried out on the edge of a thin carbon film. Since minimum contrast is located within a few tens of nanometers to zero or Gaussian focus, one can reset defocus here. Decreasing focus further to negative values will then give a reasonable estimate of the applied defocus when recording images. It should be noted that at medium resolution (Fig. 7.8b, d) reducing the size of the objective aperture will increase amplitude contrast.

To conclude this section, a few comments on advanced methods using aberration correctors and monochromators. Similar to light optics, electron microscopes suffer from lens aberrations, namely spherical (Cs) and chromatic (Cc) aberration. Both aberrations can be alleviated using correctors which are classified as being either imaging correctors (TEM, placed below the sample) or probe correctors (STEM, placed above the sample). In TEM the corrector provides the flexibility to adjust both Cs and defocus for maximum information transfer from the object wave phase into the image wave amplitude. In STEM the corrector provides the flexibility to increase the probe convergence angle, thus forming focused electron beams with sub-atomic diameters. When combining an imaging and a probe corrector into a double corrected instrument even more sophisticated experiments become possible, such as confocal electron microscopy. Finally, monochromators are used to narrow the range of electron wavelengths, which is most useful for elemental analysis and is further discussed in Sect. 7.7.

## 7.6 Electron Tomography: 3-Dimensional Imaging

One significant feature of (S)TEM imaging is that it generates in first approximation two-dimensional (2D) images, i.e. projections, of the sample. Henceforth, sample features that overlap along the electron trajectory may not be distinguishable in 2D images since NPs and their assemblies are inherently three-dimensional (3D). To overcome these limitations ***Electron Tomography (ET)*** can be employed to determine the samples 3D morphology from a set of two-dimensional projections acquired from different directions. Tomography is a very general method that is probably best known from medical diagnostics, e.g. in CAT (computer aided tomography) scans employing 2D projections of transmitted X-rays.

The general principle underlying ET, i.e. 3D reconstruction from 2D electron micrographs, is sketched in Fig. 7.9. Starting from a 3D object, e.g. NPs or an assembly of NPs, a 2D projection is acquired using (S)TEM imaging. It is important to realize that the 2D Fourier Transform (FT) of this 2D projection is mathematically equivalent to a central 2D slice through the 3D Fourier space of the object (*note*: Fourier Transform is a coordinate transform relating real space and frequency space of an object). When combining multiple projections acquired from different directions, i.e. different tilt angles, one obtains information of the entire 3D Fourier space of the 3D object. Finally, a 3D Inverse Fourier Transform (IFT) provides us a 3D image (3D intensity map) of the object. Please note that 3D reconstruction from 2D projections does not need to be carried out in Fourier space. Actually, the most

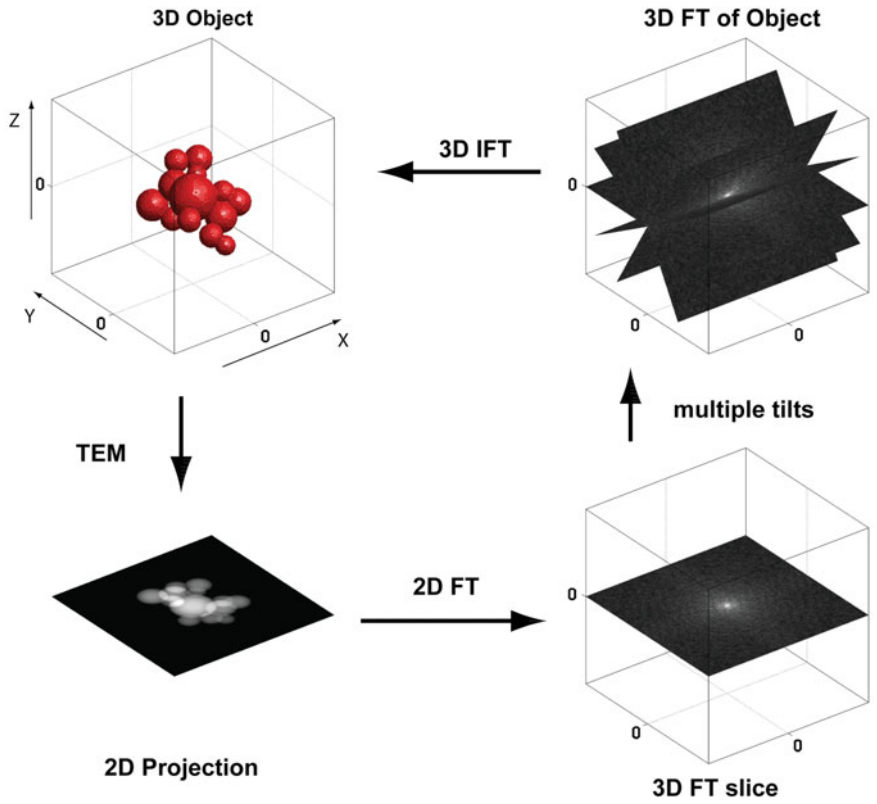


**Fig. 7.9** Principle of electron tomography, i.e. 3D reconstruction from a tilt series of 2D projections. (FT stands for Fourier Transform, IFT stands for Inverse Fourier Transform.) Reprinted with permission from Ref. [7]. Copyright (2009) American Chemical Society

common reconstruction algorithms are real space algorithms namely ***back-projection*** and ***weighted back-projection***.

From an experimental point of view, one could ask how to maximize the '3D information' one can collect from a sample. Figure 7.9 clearly shows that to achieve this one should tilt to as high as possible angles with ±90° being the optimum and to tilt the sample at as small as possible increments. This intuitive relationship has been formalized into the ***Crowther criterion*** (R = πd/N) which relates the obtainable resolution (R) to the angular increment (π/Number of images) and diameter of the reconstructed volume (d). For practical reasons, such as sample damage by the electron beam, total acquisition time, and the available tilt range of the sample holder in the microscope stage, most data acquisition nowadays covers an angular range of approximately ±70° at 1° or 2° increments. The missing angular range is often referred to as "missing wedge" of information which degrades the attainable resolution in particular along the beam direction (z-axis). Sometimes, it is possible to circumvent the missing wedge, for example when using a needle-shaped specimen

pointing into free space (think of, e.g., a carbon nanotube) that can be tilted over its own axis by 360°. Another possibility is to tilt over two axes instead of one, e.g. first x-axis and then y-axis, which is frequently used in the biological sciences. Finally, images of the tilt-series require aligning with respect to each other prior to 3D reconstruction, which, if not properly done, may cause artifacts and a subsequent loss in resolution. To summarize, the resolution of a 3D reconstruction is anisotropic: the resolution along the rotation axis (x-axis) is roughly the image resolution, that along the y-axis is given by Crowthers criterion, and that along the beam direction (z-axis) is also given by Crowthers criterion with an additional factor, often referred to as elongation factor, introduced by the maximum tilt-range.

Figure 7.10 shows an example of the unique insight provided by ET. The 2D TEM image in the left side of the figure shows two NPs that have a cross-like or star-like shape, but the 3D morphology is unclear. After performing a tilt series and a 3D reconstruction (right side), the 3D shape is completely resolved, and can be viewed from any angle. It becomes then clear that the NPs are octapods, whereby 4 pods (branches) have pointy tips, while the other 4 branches have blunt tips.

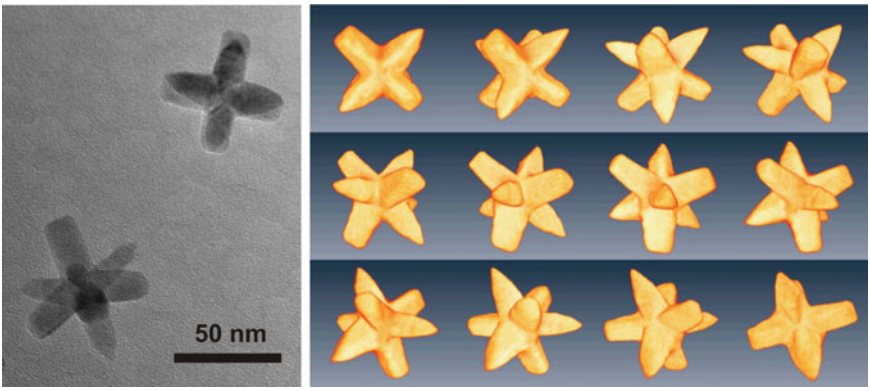


**Fig. 7.10** Octapods consisting of a CdSe core and eight CdS branches (pods). In the projection into a regular TEM image (*left*), the morphology is unclear. However, after a tomographic 3D reconstruction of a single octapod (*right*), the structure can be viewed from any angle and the shape can be analyzed in detail. Adapted with permission from Ref. [8]. Copyright (2012) Wiley

A second example, shown in Fig. 7.11, illustrates the potential of ET for the analysis of assemblies of NPs. In this example, binary NP superlattices (ordered structures of two types of colloidal NPs) have been analyzed [9]. Such structures, also referred to as metamaterials, hold promise for a series of functional materials with novel collective properties. Using ET in combination with quantitative image analysis, ambiguous interpretations based on 2D TEM could be prevented, NP sizes and superlattice parameters accurately determined, individual crystallographic point and plane defects studied, and the order/disorder at the top and bottom surfaces imaged. Furthermore, the results suggested that superlattice nucleation and growth occurred at the suspension/air interface, and even that the unit cells of some lattices were anisotropically deformed upon drying. One can imagine such detailed and

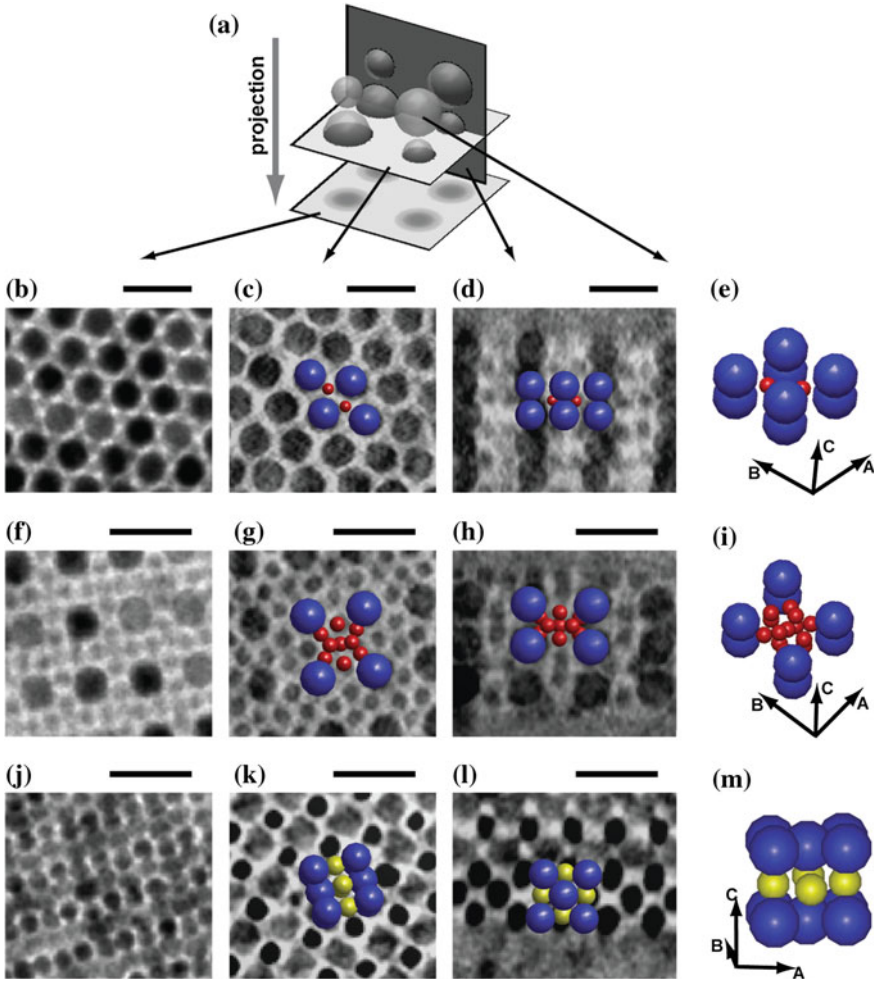


**Fig. 7.11** Crystallographic analysis of binary NP superlattices with $AB_2$, $AB_{13}$, and AB stoichiometries. **a** Cartoon explaining the relationship between the panels below. TEM image (*left*), numerical cross section through 3D reconstruction (3D intensity map) parallel to imaging plane (*left center*), numerical cross section perpendicular to imaging plane (*right center*), and unit cell showing the nanocrystal cores with lattice vectors (*right*). **b–e** $AB_2$ superlattice of 9 nm PbSe (*blue*) and 3.4 nm CdSe NPs (*red*); **f–i** ico-$AB_{13}$ superlattice of 8.8 nm PbSe (*blue*) and 3.8 nm CdSe (*red*) NPs (1/8th unit cell); **j–m** AB superlattice of 6.8 nm PbSe (*blue*) and 4.6 nm Au (*yellow*) NPs. Scale bars are 20 nm. Reprinted with permission from Ref. [9]. Copyright (2009) American Chemical Society

quantitative 3D information will be essential to understand and tune the emerging materials properties.

ET is also an essential technique for the analysis of catalytically active NPs inside porous carrier particles, e.g. to study the 3D distribution of the catalytic NPs

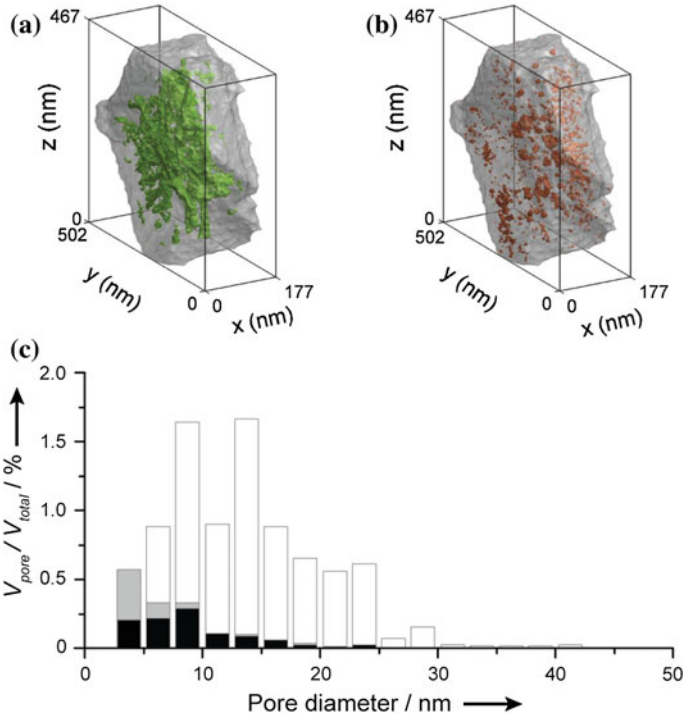


**Fig. 7.12** ET analysis of porous zeolite-Y crystallite showing open mesopores in *green* (**a**), closed mesopores in *red* (**b**), and pore size distribution quantified using image processing with open mesopores (*white*), constricted mesopores (*gray*), and closed mesopores (*black*) (**c**). Reprinted with permission from Ref. [10]. Copyright (2012) Wiley-VCH

in terms of size and inter-particle spacing. Moreover, quantitative 3D analysis of the carrier particle can provide detailed information on the pore system, as illustrated in Fig. 7.12 for a zeolite-Y crystallite. This micro-porous crystallite contains mesopores that are 2–50 nm in diameter that provide 'highways' for efficient access of reaction gases or liquids to the catalytically active sites in the zeolite framework and to the catalytic NPs. Hence the morphology of the combined system needs to be known to optimize the catalysts that produce e.g. gasoline or diesel fuels.

Now that we have become acquainted with ET, it is worthwhile to discuss in more detail that (S)TEM images are only in first approximation 2D projections of a 3D structure. From a mathematical point of view ET requires ('projection requirement') that the intensity in the image is a measure of a physical parameter of the 3D object (such as the mass thickness, or the Z number), and that it does only depend on the transmitted thickness and *not* on the direction from which the image is acquired. As seen for TEM in Fig. 7.3, if the image contrast is dependent on the orientation of the magnetite crystallites with respect to the electron beam, a 3D reconstruction will contain some artifacts. Therefore, it is important to choose wisely the imaging mode wherein the 2D projections are recorded. For non-crystalline materials (most

biological materials, glasses, etc.) or for materials which do not display much diffraction contrast such as zeolites, TEM can readily be used. In contrast, for materials which display high diffraction contrast (most crystals, metals, semiconductors), HAADF-STEM is often the preferred imaging mode, as here diffraction contrast is almost eliminated and the signal depends mainly on the atomic number of the atoms in the sample (see Sect. 7.5). Nevertheless, above observation that orientation dependent diffraction contrast of NPs in TEM does not strongly effect the tomographic reconstruction (Figs. 7.10 and 7.11) can be rationalized by the fact that diffraction contrast is only present in a few images of the tilt series, while ET averages over a much larger number of images. For more details please consult Refs. [7, 11] on ET in materials science and Ref. [12] on a direct comparison of TEM and STEM ET of the magnetite NPs shown in Fig. 7.3.

Finally, we would like to note that the availability of advanced, aberration-corrected TEMs recently made it possible to perform ***atomic-resolution tomography***. Although there are currently only a few EM groups in the world who can achieve this, it is expected that this technique will be much more widely applied in the near future, enabling e.g. atomic-scale 3D reconstruction of semiconductor-semiconductor interfaces. Furthermore, it is also possible to combine tomography with chemical mapping, which will be discussed in the following Sect. 7.7. This technique requires much effort (generating chemical maps at many tilt angles, separating the chemical elements involved, followed by a 3D reconstruction per chemical element), but provides a real 3D distribution of the chemical elements. Lastly, in ET one needs to seriously consider the beam stability of the sample so that a large number of images can be acquired without damaging the object, a point that will be further discussed in Sect. 7.8 in the context of Cryo-TEM.

## 7.7 Analytical EM: Chemical Mapping, EDX and EELS

Amongst the many interactions whereby the high-energy electrons from the electron beam interact with the electrons in the sample, there are a number of processes that can provide chemical information about the atoms in the sample. Two of these are particularly important: the emission of characteristic *X*-rays (***energy-dispersive X-ray spectrometry*, EDX**) and the energy spectrum of electrons that have lost energy as a result of their interaction with the specimen (***electron energy loss spectrometry***, **EELS**). Two such spectra, obtained on the same material, are shown in Fig. 7.13. In general, it can be stated that EDX can be used for most chemical elements but is less sensitive to light elements (e.g., B, C, N, O).

EELS works well for a number of chemical elements, but in some cases the peaks are not distinguishable from the background. It is quite suitable for most light elements, though, and is thereby complementary to EDX analysis. In addition, EELS offers the opportunity to study plasmonic properties (whereby electrons lose their energy through interactions with plasmons) and is sometimes able to distinguish

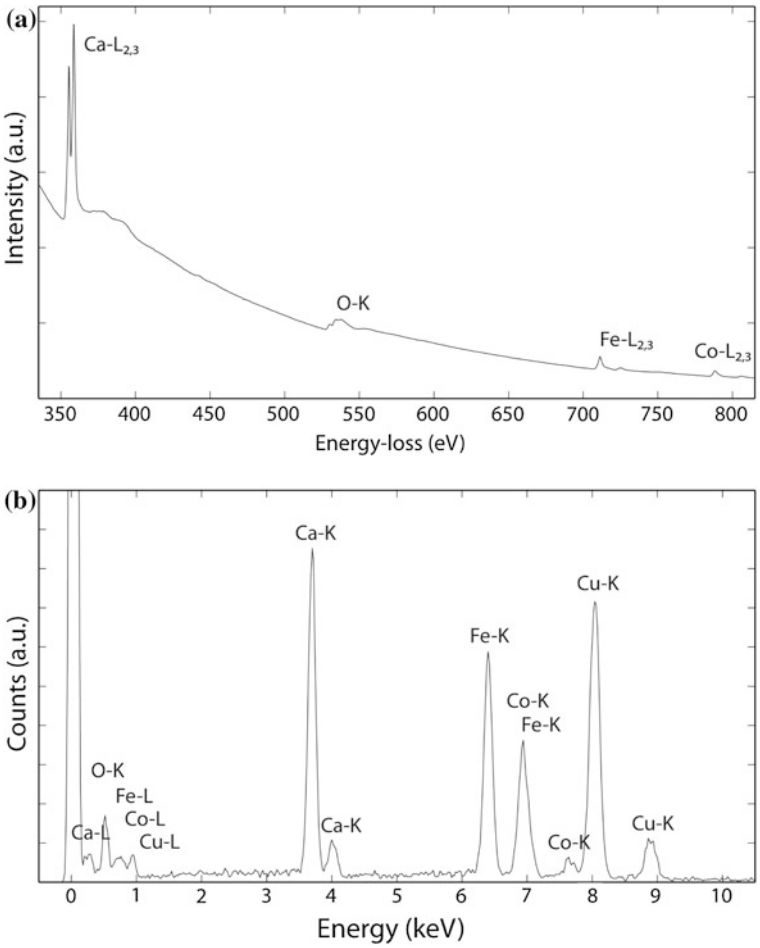


**Fig. 7.13** **a** EELS spectrum and **b** EDX spectrum obtained on the same material: $Ca_2FeCoO_5$. There are clear differences in background and detectability of the peaks. Reprinted with permission from Ref. [13]. Copyright (2012) Wiley-VCH

between different electronic or magnetic states of the atoms (e.g., distinguishing between $Fe^{2+}$ and $Fe^{3+}$, or $Mn^{2+}$ and $Mn^{3+}$). Below, we will discuss EDX and EELS into more detail.

### *7.7.1 Energy-Dispersive X-ray Spectrometry (EDX)*

Emission of a characteristic X-ray can occur after an electron from the electron beam has knocked out a core or semi-core electron from its orbit in one of the atoms in the specimen. When the vacant electronic level is filled by an electron from one

of the outer shells, the energy difference between these two electronic levels results in the emission of a photon with energies in the X-rays range. Therefore, the bombardment of target atoms with ~100 keV electrons results in the emission of many X-rays (K-, M- and L-edges in the spectra) corresponding to the filling of vacant electron levels in various electronic shells (K, L, and M shells). The energy of the X-rays is characteristic for each chemical element in the specimen. By using an electron probe (STEM mode, Sect. 7.3) and collecting an X-ray spectrum at every pixel of the image, a chemical map can be made of all atom species in the nanostructure. Such chemical maps (separate per element, and the overlapping image) are shown in Fig. 7.14 for a Au-CdSe-Au nanodumbbell and a AuS/Cd core/shell NP [14]. This technique is referred to as ***energy-dispersive X-ray spectrometry*** (abbreviated as either ***EDX*** or ***EDS***).

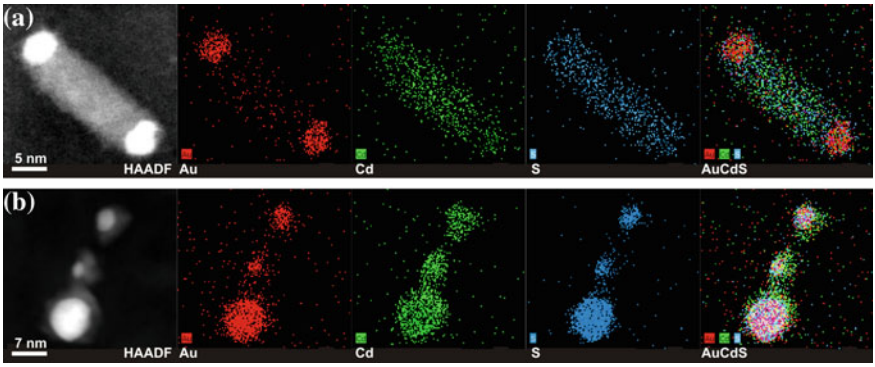


**Fig. 7.14** HAADF-STEM image and EDX chemical maps (elements Au, Cd, and S) of **a** a CdSe nanorod with Au tips and **b** AuS/Cd core/shell NPs. Reprinted with permission from Ref. [14]. Copyright (2011) American Chemical Society

Please note that separate X-ray spectra such as shown in Fig. 7.13b are collected for every individual pixel of the image, and that all of these spectra have to be analyzed with X-ray spectra fitting software to translate them into the chemical composition at each pixel position. Only when fitting of the spectra has been performed for all pixels, chemical maps such as those shown in Fig. 7.14 can be obtained.

### *7.7.2 Electron Energy Loss Spectrometry (EELS)*

While the majority of the electrons will go through the TEM specimen without having any interaction at all, a number of them will undergo elastic interactions (such a Bragg scattering, see Sect. 7.3) whereby no energy losses occur. Other electrons will undergo interactions with the target atoms whereby energy losses do occur. By analyzing the energy spectrum of the electrons that have lost energy,

certain atomic species can be identified because all atoms have a characteristic energy loss, a 'fingerprint'. This technique is referred to as ***electron energy loss spectrometry*** (**EELS**). Examples of characteristic energy loss peaks are shown in Fig. 7.13a. Please note that the peaks have a width of a few eV, which implies that an energy resolution of approximately 0.1 eV is required to resolve peaks that are in close vicinity. This is not a trivial issue, as the total energy of the electrons is typically 200,000 eV, so that the relative energy spread of the beam electrons should be approximately $10^{-6}$. This is achieved with a monochromator, which is mounted directly underneath the electron source. The mono-energetic (*monochromatic*) electron beam then passes through the specimen, whereby a fraction of the electrons undergoes energy losses due to the interaction with atoms in the sample. The resulting energy spectrum at the end of the beam line is then analyzed with an EELS detector, which employs a magnetic prism. The higher the energy of the electrons, the less they are deflected in the magnetic field, which allows collecting spectra such as shown in Fig. 7.13a.

It should be mentioned that while EDX works for almost all elements, except the lightest ones, EELS only works well for particular atomic species that have a clear 'fingerprint'. Another difficulty often encountered with EELS is that the characteristic peaks of a number of elements are broad and overlapping, which makes it difficult to resolve the spectrum. Similar to the chemical mapping using EDX in STEM mode (Fig. 7.14), also chemical mapping can be performed using EELS in STEM mode (*EELS mapping*), now by analyzing the chemical composition by fitting the EELS spectra (Fig. 7.13a).

An alternative mode for chemical mapping using EELS is called ***energy-filtered TEM*** (**EFTEM**). Here the microscope is operated not in STEM mode, but in regular TEM mode, but with an energy filter somewhere in the beam line whereby only those electrons are selected that are within a certain energy window. For example, in Fig. 7.13a an energy window can be put over the Ca-L peak, so that an image is obtained that is built only from electrons that have interacted with Ca (obviously, this requires an advanced background correction which we will not discuss here).

An example of an EFTEM image is shown in Fig. 7.15. Panel (e) shows an image of an octapod whereby the energy window is set such that only electrons with zero loss (ZL) of energy are used to create the image. Panel (f) shows two overlapping images: in red the image obtained by selecting the Cu-L peak in the EELS spectrum, and in blue the image obtained by selecting the Cd-M peak in the EELS spectrum. In these octapods (NPs consisting of a CdSe core and eight CdS legs, similar to those shown in Fig. 7.10), the tips of the pods have been chemically modified to consist of a Cu-containing compound [15]. EFTEM provides direct chemical mapping of the result of these chemical modifications. EFTEM relies on the same physical principle as EELS mapping (recording EELS spectra at every pixel in STEM mode). Nonetheless, EFTEM is in general preferred over EELS mapping because it is faster in acquisition times, although this may change in the future as EELS detectors are becoming increasingly sensitive.

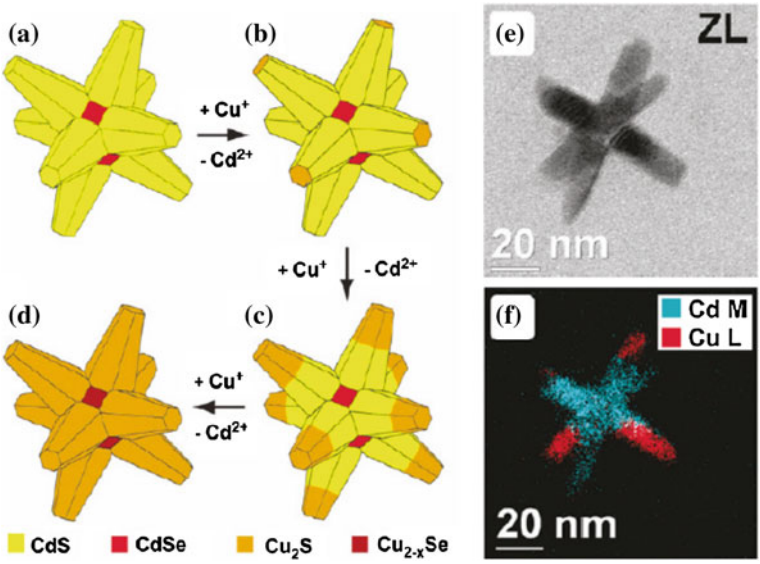


**Fig. 7.15** **a–d** Schematic of the cation exchange process whereby the CdS pods of octapod-shaped particles are transformed into $Cu_{2-x}Se$. **e** EFTEM image showing the zero-loss electrons. **f** Overlapping EFTEM images showing the Cd-associated chemical map in *blue* and the Cu-associated chemical map in *red*. Reprinted with permission from Ref. [15]. Copyright (2011) American Chemical Society

## 7.8 Cryo-TEM: Frozen-in Nanoparticles and Their Assemblies

One topic that has not been discussed so far is the preservation state of the sample. For instance, a common preparation method for solid inorganic NPs involves the drying of suspension droplets atop an electron transparent carbon support film (Sect. 7.2.1 above). In case the NPs are stabilized and do not deform upon agglomeration, no adverse effects of the sample preparation are observed.

In case of drying of a colloidal suspension the concentration of the material will increase dramatically and may drive aggregation of existing assemblies along non-equilibrium pathways. Subsequently suspended structures will be exposed to the surface tension of the solvent, potentially leading to the collapse of aggregate structures. This may cause severe misinterpretation of actually existing NP populations. To circumvent such sample preparation artifacts, colloidal NPs should be observed in their native liquid environment. To enable observation of liquid samples inside a high vacuum electron column essentially two approaches are applied: (1) using an environmental cell holder (see the next section) or (2) cryogenic preservation of a thin film of the liquid sample.

Cryo-TEM images NPs within a solidified film of the native embedding liquid, thus preserving their respective temporal and spatial arrangement. The workflow of

Cryo-TEM sample preparation by *plunge freezing* is sketched in Fig. 7.16. First, a droplet of the solution, commonly $\sim 3$ μL, is applied to a perforated carbon film. The suspension not only fills the holes in the support but also covers one or both sides of the support film (panel a). Second, the support film is pressed (blotting) from both sides with filter paper which removes all excess liquid except the one contained in the holes (panel b). When the filter paper is withdrawn, some of the liquid in the holes is also removed creating slightly convex menisci. Such thin liquid films are very sensitive to drying, thus samples need to be prepared in an environmental chamber with a saturated solvent atmosphere to minimize evaporation. Third, the sample is plunged into a cryogen (panel c), e.g. liquid ethane, which very rapidly cools the sample, thus avoiding crystallization of the liquid embedding medium. Fourth, the sample is removed from the liquid ethane bath and kept at liquid nitrogen temperature during sample transfer to electron microscope and during observation (panel d). Note that blotting may induce shear stress in the liquid and, therefore, a waiting time (seconds to minutes) can be applied between blotting and vitrification, so that the film and dispersed objects can relax into their original organization. Moreover, good wettability of the carbon support film and inert filter paper are required.

While Cryo-TEM has the unique advantage of imaging NPs in their native environment, it is also prone to misinterpretation. Some of the artifacts that may

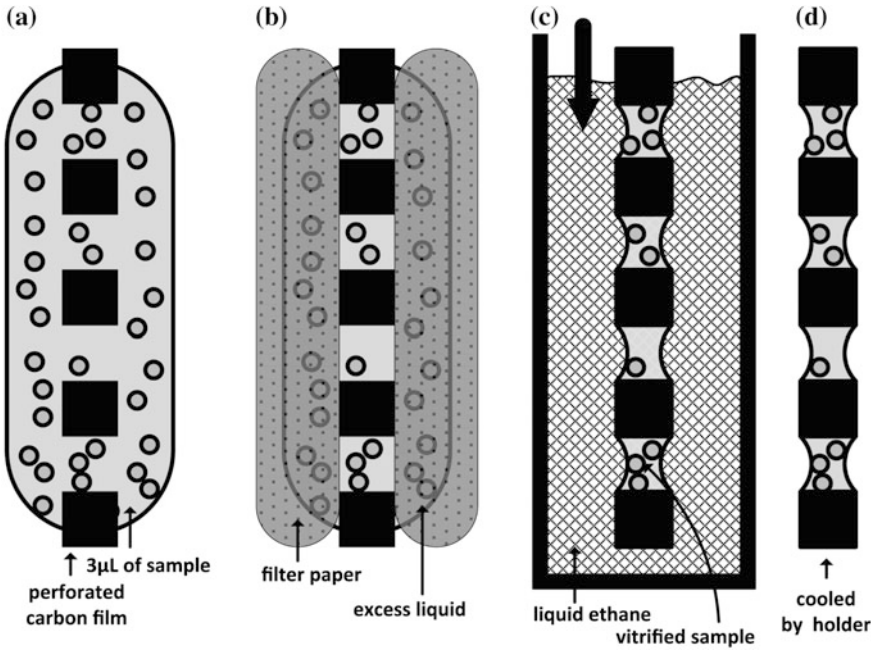


**Fig. 7.16** Workflow of plunge freezing: apply sample (**a**), blotting of excess liquid (**b**), rapid cooling (**c**), cryo transfer and imaging (**d**)

arise when trying to vitrify aqueous suspensions are displayed in Fig. 7.17. Panel (a) shows a polymer aggregate that is embedded in hexagonal ice (indicative of too low cooling speed during vitrification) appearing as dark bands throughout the image. In the case of cubic ice, high contrast objects seemingly appear as illustrated in (panel b), which is indicative of a temperature increase above −140 °C (recrystallization temperature of cubic ice) during sample transfer. Moreover, ice particulates from ambient air or contamination from the liquid ethane (see panel c) may be deposited during sample transfer to the microscope column. Finally, the most important cause of artifacts and sometimes misinterpretation is electron-beam-induced radiation damage (panel d).

All organic specimens, and under high magnification most inorganic specimens, degrade as a result of the impact of the high-energy electrons. The dissipation of the electron energy gives rise to chemical reactions and rearrangements during image

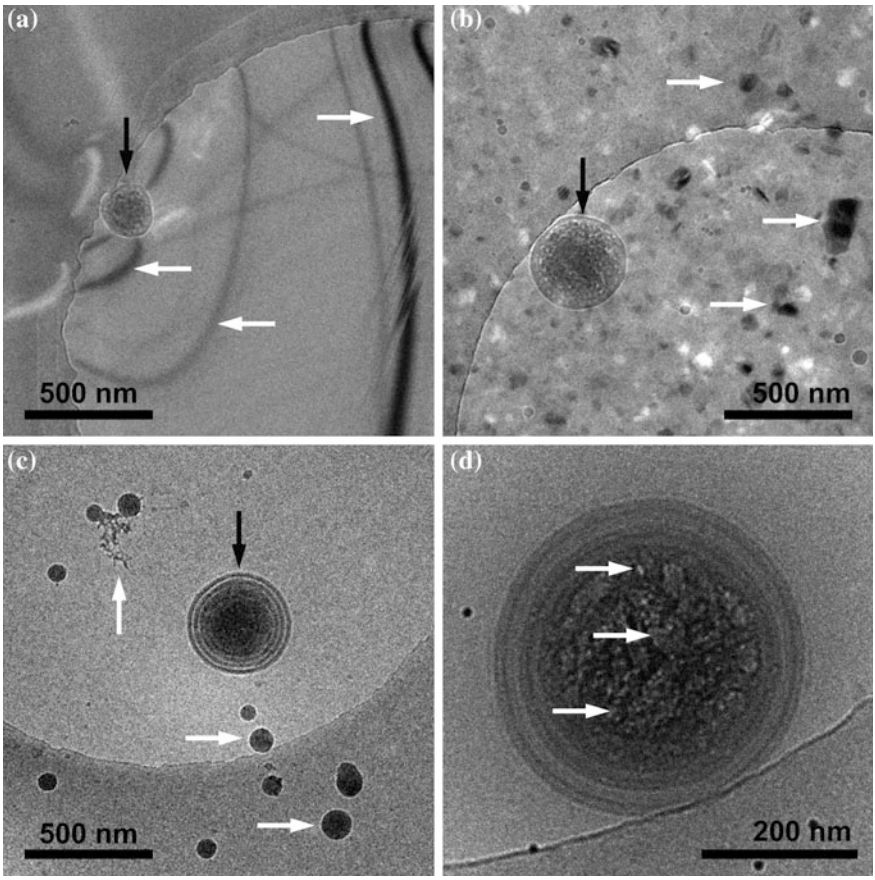


**Fig. 7.17** Polymer aggregate (*black arrows*) and Cryo-TEM artifacts (*white arrows*) showing hexagonal ice (**a**), cubic ice (**b**), ethene and ice contamination (**c**), and beam damage (**d**)

acquisition. Therefore, low-dose imaging is mandatory which utilizes a "safe" predetermined electron dose (number of electrons per square nanometer) for each image so that the required information can be extracted before the specimen is altered. For cryo electron tomography even more stringent dose requirements apply.

To conclude this section, it is worth mentioning that Cryo-TEM is a rapidly growing field of materials science. One of the driving forces is that investigations of solution borne nanostructures are extendable to organic solvents. Note that organic solvents may be even more susceptible to beam damage than water or the embedded NPs. Finally, the conclusions drawn from the experiments fully depend on the careful interpretation of the data. Hence, complicated sample preparation and advanced imaging techniques may not be required if one can establish that the observed features are without doubt the result of the solution chemistry rather than of the procedures used to obtain the images. Further details can be found in two reviews of the subject [16, 17].

## 7.9 In situ TEM: Gas Exposure and Heating

One major challenge, and a fast developing sub-field of electron microscopy, is in situ TEM: performing physical and chemical experiments *inside* the electron microscope while watching. For example, long before "nanoscience" emerged as a research field, catalytic NPs were already used in the catalysis industry, e.g. to crack hydrocarbons in oil refineries. It is possible, of course, to let these particles do their work at high temperatures and high pressures, and examine them afterwards to investigate what happened to the samples. The issue at hand is that the NPs that are studied afterwards are no longer the same NPs that were catalytically active at high pressures and high temperatures. Therefore, what is really required is to replicate these conditions inside the electron microscope.

There are many possible experiments that can be performed in the EM, for example illumination with lasers, ion beam implantation, examination of particles in liquids and fluids, passing electrical current through the specimen, exposure to magnetic fields, mechanical testing such as bending and tensile testing, correlative light and electron microscopy (CLEM) whereby a light microscope and an electron microscope are combined in one apparatus, etc. As this chapter does not intend to be exhaustive, we selected two popular in situ methods for further discussion: gas exposure and heating experiments.

### *7.9.1 In Situ Gas Exposure*

Studying NPs while being exposed to gases usually takes place in a specially designed microscope: the *environmental TEM (E-TEM)*. There is a low gas pressure ($\sim 10^{-3}$ bar) present at the position of the specimen. The presence of gas degrades

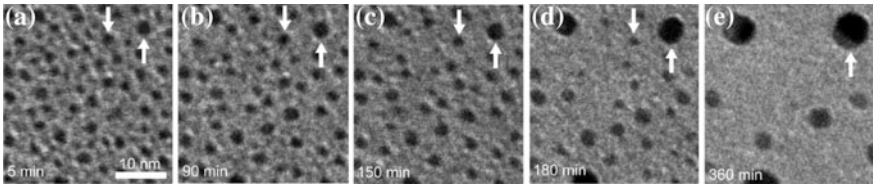


**Fig. 7.18** Pt NPs on an $Al_2O_3$ support, ripening in time under the influence of an oxygen atmosphere (10 mbar air at 650 °C). Shrinkage and growth of NPs is indicated with *white arrows* to guide the eye. Adapted with permission from Ref. [18]. Copyright (2010) American Chemical Society

the resolution of the microscope, because the electrons have to travel through a long volume containing gas molecules, where they interact with gas molecules instead of the NP under investigation. Therefore, a differential pumping system is installed which maintains the pressure in the direct vicinity of the specimen, but restores the vacuum in the rest of the column so that at the top (where the electron source is), the vacuum is of very high quality. A nice demonstration of E-TEM is shown in Fig. 7.18. Here catalytic Pt NPs supported on alumina are ripening in the presence of an oxygen-rich gas (air). During heating at a temperature of 650 °C in this environment, bigger particles grow at the expense of smaller ones. The size distribution of the particles thus obtained depends on the particular gas atmosphere [18]. While in E-TEM pressures are limited to the mbar range, much higher pressures ($\sim 1$ bar) can be obtained when using gas cells, whereby the gas is confined in a very thin volume between two membranes. In either case, there is always a risk that the electron beam creates ionizations in the gas which affect the experiments. Therefore, in E-TEM it is a standard procedure to vary the intensity of the electron beam in order to verify that it does not have a strong influence on the observations.

### *7.9.2 In Situ Heating*

As many materials are processed and manipulated by means of heating, also this in situ method is very popular. Apart from conventional heating holders whereby the whole TEM support is heated by a surrounding ceramic oven, recently microhotplates based on MEMS (microelectromechanical systems) technology have emerged as a preferred means to perform in situ heating experiments. One major issue with heating is thermal drift. The heat that is produced in the sample area, spreads to the sample holder itself (typically 30–40 cm in length), which then thermally expands. While this is a very minimal effect from a macroscopic point of view (the linear thermal expansion coefficient of most metals is in the order of $10^{-6}\,K^{-1}$), when zooming into the nanoscale this means that the specimen is moving so fast that the image is completely blurred and that high resolution is not achievable. The miniaturization of the experiment is a solution to this problem: only the direct

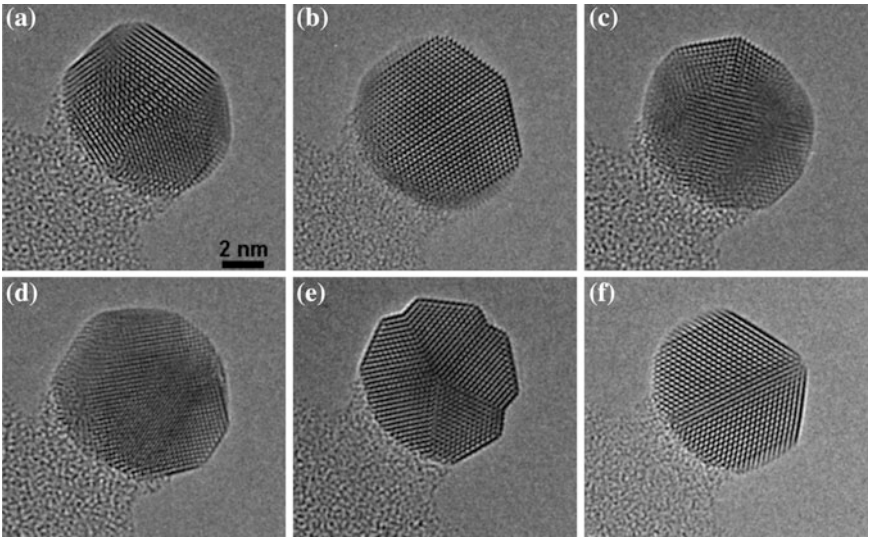


**Fig. 7.19** Heating experiment performed in the TEM, whereby a 9-nm sized Au NP transforms from one morphology at elevated temperature: 415 °C in panels (**a**–**d**), 450 °C in panels (**e**, **f**). Reprinted with permission from Ref. [19]. Copyright (2010) Elsevier

environment of the NPs is heated to a certain temperature. The total heat dissipation of this microscale experiment is so small that the heating holder itself does not heat up significantly, thereby minimizing thermal drift issues.

Figure 7.19 shows a nice example of a gold NP at an elevated temperature of approximately 450 °C. It is clear that the NP swaps from one morphology to another. Sometimes the particle displays a single crystal (panel d), but is also found in multiply twinned particle (MTP) configurations (panels a, b, c, e, f). Usually NPs will not change their morphology at room temperature: there is an energy barrier that needs to be crossed. At elevated temperatures, however, there is sufficient kinetic energy available to cross these barrier and to 'hop on the morphology-dependent energy landscape'. The lower melting points of NPs with respect to the bulk materials can also be studied in detail with these in situ experiments.

## 7.10 Outlook: Quantitative and Dynamic EM

Recent developments in the field of EM now emphasize more and more the quantitative aspect of experimentation and analysis. This means that electron microscopes have evolved from powerful magnifying tools that provide images to extremely versatile measurement devices that provide structural, chemical, electronic, or magnetic information down to the atomic scale. For example, in Fig. 7.1e above bright spots are visible that represent columns of atoms. By analyzing the

intensity of the atomic columns the number of atoms in each column was estimated. By combining the information from just three such analyses, looking at the sample from different directions, an atomic resolution 3D reconstruction of the PbSe core within the CdSe rod-shaped shell was obtained [5]: an excellent example of quantitative EM (QEM). Also the analysis of the 3D inter-particle spacing and ordering in NP superlattices (Fig. 7.11, [9]); or the determination of the pore structure and connectivity (Fig. 7.12, [10]) are examples of QEM.

A second direction of EM development that now evolves rapidly is in situ experimentation, dynamic TEM (DTEM) and ultrafast electron diffraction (UED). This means that experiments that were previously performed outside the electron microscope (ex situ) are now redesigned to be performed inside the TEM, so that structural and chemical changes during materials assembly or operation, (e.g., catalysts) can be followed in real time and under realistic application conditions. The dynamic aspect of EM is introduced by using very short electron pulses for imaging (DTEM) or diffraction (UED). Both DTEM and UED allow observing the transient behavior during e.g. a chemical reaction or a phase transformation and will in the future bring significant advance in our conception of the basic phenomena of physics, chemistry, and biology.

Furthermore, a point that has been hardly addressed in this chapter on account of size limitations, the impact of calculation and simulation methods becomes increasingly important. For instance, to analyze EELS spectra it is often required to be guided by quantum mechanical calculations which predict the 'fingerprint' of the chemical elements. Also, imaging simulations are often required to fully understand and interpret the contrast in TEM images. Finally, as the field of nanoscience and nanotechnology continues to develop from *describing* to *understanding* to *designing* [13], also TEM will develop as indispensable characterization method; its contribution cannot be overestimated.

## 7.11 Exercises

1. What would you use for imaging of nanoparticles, layers or aggregates thereof, SEM or TEM? Explain your choice depending on size, composition, and state of the material.
2. Assume you have NPs present in suspension or as a composite, i.e. embedded in a matrix such as a polymer, how would you prepare your sample for TEM or SEM? Why?
3. What would be necessary requirements for a EM sample support film? Suggest commonly used examples.
4. What kind of samples would be sensitive to charging effects by the electron beam? What solutions can you propose to resolve this issue?
5. You are given a mixture of nanoparticles and have to determine which are crystalline and which are amorphous. How would you do it? Give two alternative approaches using EM.

6. In case you do not clearly see the nanoparticles in bright-field TEM images, what can you do to increase image contrast? Can you think of three alternatives? Would you think that annular dark-field STEM imaging can help?
7. For the octapods shown in Fig. 7.10, calculate the resolution defined by the Crowther criterion (Sect. 7.5) for 3D reconstructions based on tilt series over ±60° and ±80° with increments of 1°, 2°, and 5°.
8. What would be the best way to analyze Pt NPs inside a nanoporous zeolite support (consisting mainly of Si, Al and O)? TEM or STEM? EDX or EELS? Explain why and discuss advantages and disadvantages.
9. What problems can you expect when you put a liquid sample (contained by two thin sealing membranes) in the path of the electron beam in an EM?
10. What other experiments can you think of that can be performed in situ in the TEM? What are the challenges in those cases?
11. Assume you would like to carry out a time-resolved experiment in the EM. What limits your time resolution and how could you improve it?

## References

1. Williams, D.B., Carter, C.B.: Transmission Electron Microscopy—A Textbook for Materials Science, 2nd edn. Springer, USA (2009)
2. van Tendeloo, G., van Dyck, D., Pennycook, S.J. (eds.): Handbook of Nanoscopy. Wiley-VCH, Weinheim (2012)
3. Yalcin, A.O., Fan, Z., de Nijs, B., Tichelaar, F.D., van Blaaderen, A., Vanmaekelbergh, D., van Huis, M.A., Zandbergen, H.W.: unpublished results
4. Velikov, K.P., van Blaaderen, A.: Synthesis and characterization of monodisperse core-shell colloidal spheres of Zinc Sulfide and Silica. Langmuir **17**, 4779–4786 (2001)
5. Bals, S., Casavola, M., van Huis, M.A., van Aert, S., Batenburg, K.J., van Tendeloo, G., Vanmaekelbergh, D.: 3D atomic imaging of colloidal core-shell nanocrystals. Nano Lett. **11**, 3420–3424 (2011)
6. Lenders, J., Dey, A., Friedrich, H., de With, G., Sommerdijk, N.: unpublished results
7. Friedrich, H., de Jongh, P.E., Verkleij, A.J., de Jong, K.P.: Electron tomography for heterogeneous catalysts and related nanostructured materials. Chem. Rev. **109**, 1613–1629 (2009)
8. Goris, B., van Huis, M.A., Bals, S., Zandbergen, H.W., Manna, L., Van Tendeloo, G.: Thermally induced structural and morphological changes of CdSe/CdS octapods. Small **8**, 937–942 (2012)
9. Friedrich, H., Gommes, C.J., Overgaag, K., Meeldijk, J.D., Evers, W.H., de Nijs, B., Boneschanscher, M.P., de Jongh, P.E., Verkleij, A.J., de Jong, K.P., van Blaaderen, A., Vanmaekelbergh, D.: Quantitative structural analysis of binary nanocrystal superlattices by electron tomography. Nano Lett. **9**, 2719–2724 (2009)
10. Zečević, J., Gommes, C.J., Friedrich, H., de Jongh, P.E., de Jong, K.P.: Mesoporosity of Zeolite Y: quantitative three-dimensional study by image analysis of electron tomograms. Angew. Chem. Int. Ed. **51**, 4213–4217 (2012)
11. Midgley, P.A., Dunin-Borkowski, R.E.: Electron tomography and holography in materials science. Nat. Mater. **8**, 271–280 (2009)

12. Friedrich, H., McCartney, M.R., Buseck, P.R.: Comparison of intensity distributions in tomograms from BF TEM, ADF STEM, HAADF STEM, and calculated tilt series. Ultramicroscopy **106**, 18–27 (2005)
13. Van Tendeloo, G., Bals, S., Van Aert, S., Verbeeck, J., Van Dyck, D.: Advanced electron microscopy for advanced materials. Adv. Mater. **24**, 5655–5675 (2012)
14. van Huis, M.A., Figuerola, A., Fang, C.M., Béché, A., Zandbergen, H.W., Manna, L.: Chemical transformation of Au-tipped CdS nanorods into AuS/Cd core/shell particles by electron beam irradiation. Nano Lett. **11**, 4555–4561 (2011)
15. Miszta, K., Dorfs, D., Genovese, Al, Kim, M.R., Manna, L.: Cation exchange reactions in colloidal branched nanocrystals. ACS Nano **5**, 7176–7183 (2011)
16. Friedrich, H., Frederik, P.M., de With, G., Sommerdijk, N.A.J.M.: Imaging self-assembled structures: the interpretation of TEM and cryo-TEM images. Angew. Chem. Int. Ed. **49**, 7850–7858 (2010)
17. Cui, H., Hodgdon, T.K., Kaler, E.W., Abezgauz, L., Danino, D., Lubovsky, M., Talmon, Y., Pochan, D.J.: Elucidating the assembled structure of amphiphiles in solution via cryogenic transmission electron microscopy. Soft Matter **3**, 945–955 (2007)
18. Simonsen, S.B., Chorkendorff, I., Dahl, S., Skoglundh, M., Sehested, J., Helveg, S.: Direct observations of oxygen-induced platinum nanoparticle ripening studied by in situ TEM. J. Am. Chem. Soc. **132**, 7968–7975 (2010)
19. Young, N.P., van Huis, M.A., Zandbergen, H.W., Xu, H., Kirkland, A.I.: Transformation of gold nanoparticles investigated using variable temperature high-resolution transmission electron microscopy. Ultramicroscopy **110**, 506–516 (2010)